ZnO Quantum Dots-Graphene composites: Formation Mechanism and Enhanced Photocatalytic Activity for Degradation of Methyl Orange Dye

Ahmad Tayyebi[1], Mohammad outokesh[1*], Meysam Tayebi[2], Azizollah Shafikhani[3], S. Sevinç Şengör[4]

[1]Department of Energy Engineering, Sharif University of Technology, Azadi Ave. P.O. Box: 113658639, Tehran, Iran.

[2]Chemical Engineering Department, Faculty of Engineering, Ferdowsi University of Mashhad

[3]Departmentof Physics, AlZahra University, Tehran, 1993893973, Iran.

[4]Southern Methodist University, Department of Civil and Environmental Engineering, Dallas, TX 75275, USA

*Corresponding author's email address: Outokesh@sharif.edu

Abstract: The current study demonstrates homogenous decorating of zinc oxide quantum dots (QDs) onto graphene oxide (GO) surface *via* simple chemical method. The AFM image exhibited that the prepared graphene was 0.8 nm thick and hence practically monolayer. Average size of the ZnO QDs was estimated by transmission electron microscopy around 3 nm. Instrumental and chemical analyses demonstrated formation of a strong bond between ZnO QDs and GO, through C-O-Zn and C-Zn bridges. The UV-visible spectra displayed that the introduction of graphene sheets to ZnO QDs resulted in higher absorption intensity of UV as well as widening of adsorption window toward visible light for ZnO-Graphene due to chemical bond between ZnO QDS and graphene surface. Results showed that adding of graphene up to 30% can improve resistance of ZnO against acids however for keeping the activity of catalyst, the recommended pH is near neutral (pH ≈6-7.2). In addition, the presence of graphene on the surface of the ZnO could significantly suppress the photocorrosion effect. The ZnO-Graphene hybrids indicated enhanced photocatalytic activity for degradation of methyl orange (MO) with the following order: ZnO-5% Graphene > ZnO-10% Graphene > ZnO QDs > ZnO30% -Graphene. This enhancement of photocatalytic activity may be attributed to the extended absorption of visible light, reducing of electron-hole recombination rate, and adsorption of MO molecules onto the huge surface area of graphene, where they are kept at vicinity of ZnO for decomposition.

Keywords: ZnO-Graphene; Enhanced photocatalysis; Formation mechanism; Visible photocatalytic activity, Photocorrosion

Introduction. Recent global warming that has decreased the amounts of atmospheric precipitations in some geographical areas, accompanied with the rapid growth of the world population, has raised concern about depleting of the clean water resources[1]. Thus, treatment, and reuse of wastewater has become an important global issue. Between the three types of wastewater, namely industrial, agricultural and municipal, the first one is the easiest to treat, because in any kind of industry, number of the chemical agents that pollute the water is limited. Nowadays, in industrialized countries, post processing of the waste water is commonplace, because the rate of production of the effluents is gigantic, and the environmental concern adds to the significance of the problem[2].

As for treatment of the industrial effluents, so far, a great deal of technologies has been devised[3]. One of the finest techniques for decontamination of the wastewater, which recently has attracted much interests is photo-degradation of the toxic pollutants by nanocatalysts[4]. Up to now, several metal oxide semiconductors have been tested as photocatalyst for this purpose, including: TiO_2, SnO_2, WO_3, Fe_3O_4, and eventually ZnO [5-7]. Among these materials, zinc oxide presents numerous advantages such as: availability, non-toxicity, cost efficiency, and thermal stability [8]. As regard to only being active in the UV region of the solar light, and thus absorbing only 5% of the sunlight energy, extending of the band gap of ZnO into the visible region, and hence improving of its photocatalytic efficiency is of great importance[9, 10]. One of the suggested methods for this purpose is decorating of ZnO nanoparticles (NPs) on a substrate with high surface area such as zeolite, nanoclay or carbon-based materials [11-13]. The aforementioned carbon-based materials are divided into two categories:1-Conventional, including graphite, carbon black, and activated carbon which have been studied extensively, and 2- New family comprising carbon nanotube (CNT), fullerenes, and most recently graphene. Since their emerges in the past few years, the new family have presented themselves as attractive hybridizing agents for synthesis of photocatalysts owing to their exceptional electronic properties, and the adsorption capacity[14-16].

Graphene starred for the first time in the scientific sky in 2004[17] and due to its unique electronic, optoelectronic, and physical properties, opened new windows in synthesis of advanced

materials. Graphene-based hybrids have been widely employed in various applications including polymer-composite[18], drug delivery[19], sensor fabrication [20], catalysis[21], and nanoelectronic[22].

Currently, most of the graphene derivatives (G-Ds) are prepared from graphene oxide (GO) as the starting material. This is due to the fact that GO is an intermediate material in the synthesis of graphene, and its usage can shorten synthesis time of the G-Ds considerably[23]. Graphene oxide is a lamellar material with epoxy (C-O-C), hydroxyl (OH), and carboxyl (COOH) groups, that its groups can act as nucleation sites for growth of semiconductor nanoparticles[24]. Recently, graphene-based semiconductor photocatalysts have received a great deal of attention owing to their high catalytic performance[25, 26]. Moreover, due to the existence of oxygen functionalities on its surface, and the enormous surface area, deposition of semiconductors NPs on the GO is homogeneous[27]. Furthermore, Deposition of the nanoparticles on the GO also prevents restacking of the graphene sheets during post-reduction of the GO[28].

So far, several researchers investigated synthesis of ZnO-Graphene hybrid for different applications. Nearly in all of those works, ZnO-Graphene showed an enhanced activity compared to the pristine ZnO[8, 14, 29]. Bai and coworkers synthesized ZnO-Graphene using in-situ reduction of graphene oxide and utilized it for photo degradation of methylene blue. The hybrid showed 4.6 times higher efficiency under visible light compared to pure ZnO[14]. Lv et al. prepared ZnO-Graphene-CNT triple composite to improve the low electric conductivity of the ZnO-Graphene hybrid. Under UV irradiation, the new composite showed a maximum degradation efficiency equal to 96%, which was higher than that of the ZnO-Graphene hybrid (88%)[30]. Because of the efficient electron-hole separation, notable electron conductivity, and high surface area of graphene as substrate, incorporation of graphene and semiconductors in a composite is turned out to lead to conspicuous photocatalytic activity.

Semiconductor quantum dots (QDs) present size-dependent band gap shift[31] resulting in interesting optical properties due to the quantum confinement effect. The smaller ZnO NPs are, and

the narrower size distribution they have, the higher surface for catalytic reaction they achieve, and the wider band gap and photocatalytic performance they attain[32]. Zubir et al. and Song et al. proposed that ZnO QDs are decorated on the surface of GO via covalent connection between Zn^{2+}(ZnO) or Zn^{2+} and oxygen functionalities on the surface of GO[33]. Hsiao et al. showed that the functional groups can be efficiently grafted onto surface of graphene sheets using epoxy ring-opening reaction[34]. Wang et al. demonstrated that metal oxide may not be grafted onto pristine graphene unless surface functionalization was provided beforehand [35]. Ma et al. found that dangling bonds and defects on the surface of graphene could act as a bridge between ZnO and the graphene sheet[36]. Despite great deal of attempts that have been made for clarification of mechanism of anchoring of ZnO onto graphene surface, there is still a paucity of reliable information about this linkage.

The current study is aimed at synthesis of the ZnO-Graphene composite with the ZnO particles in the range of few nanometers, elucidation of their formation mechanism, and application of the obtained composite for photocatalytic degradation of methyl orange. The study particularly intends to investigate widening of the band gap of ZnO QDs from UV to visible region, when it is compounded with graphene.

2. Experimental Methods

2.1. Materials. Natural flake graphite, sulfuric acid (98%), hydrochloric acid (37%), hydrogen peroxide (30%), sodium nitrate, anhydrous dimethyl formamide (DMF), zinc acetate and potassium permanganate were purchased from Merck, AG, Germany and used without purification.

2.1. Preparation of graphene oxide. Graphene Oxide was prepared from highly pure graphite using the modified Hummers method [37]. In a typical procedure, a mixture of 2 g graphite powder and 2 g sodium nitrate was dispersed in 45 cm^3 of 95% (w/w) sulfuric acid. While the temperature was maintained below 5 ^{0}C using ice bath, 6 g potassium permanganate was gradually added to the

dispersion within 2 h. Then the mixture was stirred for 30 min, and 100 mL distillated water was slowly added to it. At this stage, temperature was increased to 95 ^{0}C, and the mixture was maintained at that temperature for another 30 min. Afterward, the hot mixture was cooled down to 40 ^{0}C by adding 300 mL distillated water, and reaction was terminated by using 20 mL of a 30% (w/v) hydrogen peroxide solution. The obtained mixture was filtered, washed with diluted HCl to remove metal ions, and repeatedly washed (with distilled water) and centrifuged until the pH become 5. Finally prepared GO was dried at ambient temperature.

2.2. Synthesis of ZnO-Graphene composite. ZnO-Graphene hybrid with different amount of graphene was synthesized by slight modification of Son et al. method[33]. The procedure was started by uniform dispersion of calculated amount of GO in 100 mL DMF by the aid of ultrasonication (Elmasonic, S 30H, country) for 15 min to prepare 5, 10, and 30% of graphene in ZnO-Graphene composites. Simultaneously, 1 g of zinc acetate was dissolved in a mixture of 100 mL DMF and 20 mL deionized water. The GO solution then was gradually mixed with zinc acetate solution by stirring. The obtained mixture was then heated to 95 ^{0}C and maintained at that temperature for 5 h. During this period, the color of the formed ZnO-Graphene hybrid was altered to white-greyish. The mixed solution was then repeatedly washed with ethanol, and finally with water. The ZnO-Graphene composite was obtained by drying of the final centrifuged product at 55 ^{0}C.

2.3. Characterization. Morphological images of the GO nanosheets and ZnO-Graphene composite were obtained by means of low and high-resolution transmission electron microscopy (TEM / HRTEM, JEOL, JEM-2100, Japan). The employed HRTEM also supported the selected area electron diffraction (SAED) analysis. Evidence for complete exfoliation of the graphene (i.e. formation of single layer product) was provided by atomic force microscopy (AFM, Park Scientific CP-Research model, VEECO) which worked in the tapping mode, with frequency of 320 kHz, and

by using a 20 nm thick silicone tip. Samples for AFM imaging were prepared by drop casting of a dilute GO suspension (0.01 mg/mL) onto a cleaved mica substrate.

The current study exploited five methods for identifying of the chemical and crystallographic structure of the prepared materials. The first method was Raman spectroscopy (SENTERRA, BRUKER, Germany) that was performed at room temperature by a 532 nm Nd-YAG excitation laser. The second technique was energy dispersive X-ray analysis (EDX, JEOL, JEM-2100, and Japan) which provided the elemental analysis of the samples. The X-ray photoelectron spectroscopy (XPS) as the third technique revealed the chemical states of the GO before and after its reduction to graphene. The XPS instrument was equipped with a hemispherical analyzer for data acquisition, and an Al K_α X-ray source operated at pressure below 10^{-7} Pa. The XPS peaks were fitted by Gaussian components model after Shirley background subtraction. Two other employed analysis techniques included X- ray diffractometry (Rigaku Miniflex XRD, Texas, USA), and Fourier transforms infrared spectroscopy (FTIR, Perkin-Elmer, Spectrum RX, USA).

Optical characteristics of the GO suspension (0.01 mg/cm^3) were studied by a UV-Visible spectrophotometer (Perkin Elmer UV-Vis-NIR model Lambda 950) in the wavelength range of 200–700 nm.

In order to study the thermal stability and composition of prepared materials, thermo-gravimetric analysis (TGA) was performed under air atmosphere (TGA/DSC 1, METTLER TOLEDO, Switzerland). A heating rate of 10° C /min was utilized.

2.4. Chemical Stability and Sedimentation Measurements: Dissolution of ZnO QDs and ZnO-Graphene with different amount of graphene was investigated in a glass reactor at room temperature and different pH values including acidic (pH 1.0), mildly acidic (pH 3.0), neutral (pH 6.0-7.2), and neutral media (pH 7.1). For this reason, same amount of samples (0.1 gr/L) of ZnO QDs, ZnO-5% Graphene, ZnO-10 % Graphene, and ZnO-30% Graphene were dispersed in water solution and after 15 min ultrasonication at different time, sample were collected from supernatant.

The solid component was removed by 0.2 µm membrane filter and centrifugation process. The concentration of Zinc (Zn^{2+}) ions was measured by a Varian atomic adsorption spectrometer (AAS).

The stability of obtained materials at pH 7 was determined by monitoring sedimentation by a Perkin-Elmer Lambada20 UV-vis spectrometer. The change in the optical absorbance at 375 nm was obtained as a function of time.

2.5. Kinetics of the MO Adsorption. Batch-mode adsorption kinetics of MO by ZnO QDs and ZnO-Graphene were studied by adding 10 mg of each adsorbent to 10 mL of a 20 ppm MO solution that was placed in a conical flask. Samples of the solution were withdrawn at different time interval, and analysed by UV-visible spectrometer (Perkin Elmer UV-Vis-NIR model Lambda 950). The temporal loading of MO onto adsorbent was obtained from the following relation:

$$q_t = \frac{(C_0 - C_t)\,V}{m} \qquad (1)$$

where C_0 (ppm) and C_t (ppm) show concentration of the MO at time zero and time "t, min ", V (mL) stands for volume of the solution, and m (g) is the mass of the adsorbent.

2.6. Photocatalytic activity. The photocatalytic activities of ZnO QDs and ZnO-Graphene were studied by examining degradation rate of Methyl Orange (MO), in the presence of the above adsorbents under ultraviolet (UV) and visible light irradiation. The photocatalysis experiments were carried out in an open wide glass reactor using a high-pressure 100 W mercury lamp (B 100 AP, UVP) with the wavelength of 365 nm as the UV source, and a 175 W metal halide lamp (λ >420 nm) as the visible light supplier. Both of the lamps were placed 10 cm away from the reactor. About 50 mg of ZnO QDs or ZnO-Graphene was dispersed in 100 mL of a 1.5×10^{-4} M aqueous

MO solution (pH=6.5). Prior the lightening of the lamps, suspensions were magnetically stirred for 30 min in dark to attain the adsorption-desorption equilibrium. At this moment, concentration of MO was assigned as C_0. After onset of the irradiation, 3 mL of liquid was withdrawn in each time interval, and analysed by a UV-visible spectrometer (Perkin Elmer UV-Vis-NIR model Lambda 950).

3. Result and Discussion. Figure 1a shows AFM image of the GO on a freshly cleaved mica surface. The height profile of the line marked in the AFM image indicates monolayer graphene sheets with 0.8 nm thickness. It is widely accepted that due to the presence of oxygen functionalities on the surface of GO, its thickness is around 0.8-1.1 nm, which is somewhat thicker than the 0.4 nm thickness of graphene sheet[38]. Figure 1b displays the TEM image of the GO in which wrinkling and overlapping of the sheets is evident. Transparent areas in this figure exhibit monolayer graphene. Existence of six resolved spots in each depicted ring, is a clear indication of the hexagonal lattice of graphene in SAED pattern of GO in inset Figure 1b.The UV absorption spectrum of GO in Figure 1c reveals a distinct peak at 231 nm corresponding to π-π^* transitions for aromatic C-C and a shoulder at 302 nm assigned to n-π^* transitions of C=O bonds[39].

Figure 1

3.1. Morphology. Figure S1 in supplementary information shows low magnification TEM image of ZnO-Graphene and corresponding EDX analysis in which the materials compositions of both ZnO and graphene phases are depicted.

Low magnification TEM image of ZnO-Graphene is displayed in Figure 2a, in which the border of the graphene sheet is marked by the dashed red line. The ZnO QDs are homogenously distributed on the surface of graphene with average size of 3 nm (From histogram of Figure S2 in supplementary information). The homogeneity of ZnO distribution can be attributed to the presence

of enumerable oxygen functionalities on the surface of GO, which provide anchoring sites for immobilization of the ZnO QDs.

Inset Figure 2a shows the amorphous nature of graphene sheets and single crystalline structure of ZnO QDs by unresolved SAED pattern of the former and cubic SAED pattern of the latter, respectively.

Figure 2

Figure 2b shows HRTEM image of ZnO QDs, being decorated on the graphene nanosheets. Measured lattice spacing of d_{011}=0.28 nm[40] and d_{002} = 0.34 nm are consistent with the interplanar spacing of ZnO and graphene, respectively. Inset Figure 2b exhibits HR-TEM image of single ZnO QDs in which interplanar spacing in the crystal petals is 0.28 nm which corresponds to the distance between two (011) planes of hexagonal ZnO phase. Figure 2c demonstrates ZnO-Graphene quasi-core shell QDs in which hexagonal lattice of graphene shown in high magnification image.

3.2. Physical and Chemical Characterization: The X-ray diffraction (XRD) patterns of the GO, graphite, and ZnO-Graphene are depicted in the Figure S3. The XRD peak of GO shifted toward lower angles relative to the graphite as a result of intercalation of water and oxygen functionalities between graphitic layers in the GO. All characteristic peaks of ZnO exist in the XRD pattern of ZnO-Graphene. Thus, it is turned out that ZnO QDs in their pure form are deposited on the graphene (JCPDS 36-1451). An interesting point regarding the XRD pattern of ZnO-Graphene is absence of any peaks of GO or graphite in it. This phenomenon can be explained by considering the fact that in preparation of the GO specimens for XRD experiments, some sort of stacking of the layers takes place that brings about the GO peaks; whereas in ZnO-Graphene, the ZnO particles prevent restacking of the GO layers.

Raman spectroscopy was exploited to identify 1: Type of the carbon hybridization, 2: The degree of lattice disorder, and 3: Average domain size of hexagonal sp^2 ring in the graphite-like materials[41]. The I_D/I_G ratio in Raman spectra indicates the amount of defects and disorders that

are correlated to the sp^2/sp^3 ratio. As shown in the Figure 3a, I_D/I_G ratio in GO is higher (I_D/I_G =1.52) than graphite, because oxidation process during Hummers method increases the size of sp^3 domain. However, this ratio decreased noticeably in ZnO-Graphene implying that anchoring of ZnO QDs on the surface of graphene decreased the sp^3/sp^2 ratio. To further investigate the structural aspects of the materials, the experimental data were fitted by Gaussian fitting curves for identification of the peak positions and full width of half-maxima (FWHM) of D, G, and 2D bands (Figure S4a,b, and c in supplementary information). The FWHM of the D band was used as an indicator of the degree of the crystallinity. In this regard, the FWHM of the D band for graphite and GO were found to be 86 and 107 (cm^{-1}), respectively; whereas for the ZnO-Graphene it was reduced to 63 cm^{-1}. This attenuation indicates that grafting of ZnO QDs on the surface of graphene using C-O-Zn bonds decreases the degree of crystallinity of the graphene, an effect that was previously observed in Figure 3a, in which the characteristic peaks of GO and graphite disappeared in the XRD pattern of ZnO-Graphene (see discussion of the previous paragraphs). Apparently, we are facing with two contradictive phenomena as follow

1: The sp^3/sp^2 ratio obeys the following order: GO > ZnO-Graphene> Graphite

2: Crystallinity represents a different arrangement: Graphite > GO > ZnO-Graphene

If one accepts that during deposition of ZnO QDs on GO, most of the oxygen functionality of the GO are removed, the reason for decreasing sp^3/sp^2 ratio in ZnO-Graphene is found. On the other hand, our perception of the crystallinity is closely related to: stacking of graphene layers for forming a multilayered materials. Thus, the material with fewer layers presents lesser crystallinity. Since ZnO QDs prevent pill up of the graphene layers even in the solid form (i.e. specimen for Raman or XRD tests), the number of layers and hence crystallinity of ZnO-Graphene is minimum in the above series.

Figure 3

Thermogravimetric (TG) analysis was utilized to study thermal stability of the prepared materials as well as of the evaluating of their ZnO and graphene contents. The TG curve (Figure

3b) illustrates three major weight losses for the GO. The first one, an 8% weight loss up to 110 °C corresponds to the absorbed water on the GO nanosheets. The second weight loss at 225^{o}C (30%) is attributed to the loss of CO and CO_2 from the decomposition of the oxygen-containing functional groups. The third and the main weight loss (50%) of GO refers to oxidation of carbon atoms at high temperature and in the presence of air. The TG curve of RGO demonstrates just one major weight loss (65%) which is attributed to the oxidation of carbon atoms. In the case of ZnO QDs, a single weight loss occurs around 250 °C which corresponds to removing of the volatile organic functional groups from surface of the ZnO QDs. The ZnO-Graphene hybrid with different graphene content depict all of the above-mentioned weight losses including those corresponding to oxygen-containing functional groups, volatile functional groups, and carbon oxidation. Measurement of carbon oxidation in the ZnO-Graphene hybrid is an effective method to evaluate the carbon content and consequently graphene loading percentage in ZnO-Graphene. In this regards, ZnO-5% Graphene, ZnO-10% Graphene, and ZnO-30% Graphene in this study denote ZnO-Graphene hybrid with 5, 10, and 30% of graphene loading, respectively. Unless otherwise stated, ZnO-Graphene refers to ZnO-5% Graphene in this paper.

The FTIR spectra of GO and ZnO-Graphene are shown in Figure 3c. The successful oxidation of graphite in Hummer's method is affirmed by existence of different oxygen signatures in FTIR spectrum of the GO. In the case of ZnO-Graphene, most of the oxygen functionalities were removed except Zn-O stretching peak at 470 cm^{-1} and C-O vibration one at 1400 cm^{-1}. The aforementioned Zn-O peak was kept because only one crystal layer in the bottom of ZnO NP is connected to the graphene surface and the other (i.e. upper) layers can hold the ZnO crystal structure. The C-O peak on the other hand was kept because it was involved in linking of Zn to the GO through C-O-Zn bonding [29].

The chemical state and surface composition of GO and ZnO-Graphene were investigated by XPS analysis. For this purpose, the binding energies obtained by XPS analysis were standardized using carbon peak at 284.8 eV as a reference. Full scan survey of GO and ZnO-Graphene

demonstrates main characteristic peaks of C, O, and Zn apart from O and Zn auger peaks in Figure 3d [42].

In order to better survey the effect of ZnO deposition on the deoxygenation of GO, a comparison was made between deconvoluted C1s XPS spectra of the GO and ZnO-Graphene. The binding energy locations and surface area under the curves for each peak are assigned in the Figures 4a and b. As it can be seen, there are two obvious differences between the C1s peaks of GO and ZnO-Graphene. First, higher C/O ratio of ZnO-Graphene compared to the GO, due to the reduction of GO as a result of grafting of ZnO QDs on the surface of GO (Table 1), and second, emerging of C-Zn, C-O-Zn, and pi-pi peaks in ZnO-Graphene hybrids implying that ZnO QDs are bonded to the surface of graphene sheets.

In order to quantitatively evaluate the surface concentrations of carbon-bonded functional groups, the peak area of oxygen-containing bonds and C/O ratio were calculated and inserted in Table 1. The relative concentration of the oxygen functional groups on the surface of ZnO-Graphene is lowered by about 40% in comparison to pristine GO.

Figure 4

Table 1

3.3. Connection mechanism: Comprehending of detailed formation mechanism of the ZnO QDs on the surface of GO, and recognizing of the nature of chemical bonds between GO and ZnO QDs are difficult tasks. In an effort for embarking on these issues, Son et al. suggested that ZnO QDs are connected to the surface of graphene through C-O-Zn bonding[33]. However, they didn't provide a supportive evidence for their suggestion. Although, strong connection of C-O-Zn bonds between flower-like three-dimension (3D) microstructures of ZnO and reduced graphene oxide reported[15], however, there are several differences between this and Song et al. such as synthesis method, ZnO structure and the size nanostructure. The current study is to deal with the above-mentioned issues by means of O1s, and Zn2p XPS peaks fitting by component Gaussian. The XPS peaks corresponding to Zn(2p) core level of ZnO QDs is shown in Figure S5 in supplementary

information, in which Zn2p energy level is divided into two distinct levels of $Zn2p_{3/2}$ at 1023 eV and $Zn2p_{1/2}$ at 1046 eV[43]. As it can be seen, the energy splitting is around 23 eV, which corresponds to spin-orbit coupling and is within the standard reference value of ZnO. It must be noticed that the peak position of the Zn(2p) core level in ZnO-Graphene composites was shifted to higher binding energy (1.2 eV) indicating the presence of new chemical bonds between ZnO QDs and carbon or oxygen functionalities. To further elucidate the issue, $Zn2p_{3/2}$ was fitted and embedded in Figure S6 with two component Gaussians at around 1022 eV and 1022.8 eV that correspond to C-O-Zn and Zn-O, respectively.

Figure 5

In addition, we exploited O1s peak as a reactive site on the graphene surface, to shed more light on the connection mechanism. The broad and low intensity O1s peak of ZnO-Graphene relative to GO is possibly attributed to the change in the number of chemical bonds of oxygen atoms in ZnO-Graphene [43]. Indeed, due to some sort of chemical interaction (bonding) between Zn^{2+} and oxygen-containing groups on the surface of GO, the full width at half maximum (FWHM) of O1s peak is enlarged in ZnO-Graphene [44]. To prove the presence of new chemical bonds in ZnO-Graphene composites, O1s spectra of GO and ZnO-Graphene are deconvoluted and shown in Figure 5a, and b. In Figure 5a, the O1s peak of GO includes two spectral peak appeared at 531.7 and 532.8 eV, attributed to C=O (Carbonyl and Carboxyl) and C-O (Epoxy and Hydroxyl) respectively [45]. The O1s spectra of ZnO-Graphene are fitted to four component Gaussians at 529, 530.5, 531.7, and 532.8 (Figure 5b). The emerging peaks at 529 and 530.5 eV are attributed to Zn-O and C-O-Zn bonds respectively.

With the information obtained from curve fitting of C1s, O1s, and Zn 2p in hand, we are now able to put together a qualitative picture of the connection mechanism of ZnO QDs to the surface of graphene. The existence of different dangling bonds or functional groups on the surface of GO such as COOH, C-OH, and C-O-C, act as good nucleation sites to uniformly deposit ZnO QDs on the surface of graphene sheet. These functional groups immobilize Zn^{2+} ions through C-O-

Zn bonds, thereby through condensation reaction, remaining Zn^{2+} can be connected to these nucleation sites and ZnO QDs grow on these sub-layers via normal ionic bonds.

Figure 5c is a schematic illustration demonstrating how oxygen-containing groups of GO provide nucleation sites for ZnO QDs to link them to the surface of graphene. As it can be noticed, Zn^{2+} in the form of $Zn(OH)_2$ is connected *via* a ring opening mechanism by epoxy group and condensation mechanism to carboxyl and hydroxyl groups on the surface of GO[33].

3.4. Chemical stability of the prepared catalysts: Due to instability of zinc oxide in acidic media, it is important to evaluate the stability of the ZnO QDS and ZnO-Graphene hybrid in pHs<7, where it is supposed to be utilized. Dissolution of ZnO in acids is presented by the following reactions:

$$ZnO_{(s)} + 2H^{+}_{(aq)} \longleftrightarrow Zn^{2+}_{(aq)} + H_2O_{(l)} \qquad (2)$$

$$ZnO_{(s)} + H^{+}_{(aq)} \longleftrightarrow Zn(OH)^{+}_{(aq)} \qquad (3)$$

The pH of the solution plays a major role in the extent and velocity of the ZnO QDs dissolution. In order to elucidate such effects, three different quantum dots including bare ZnO, ZnO-5% Graphene, and ZnO-30% Graphene were selected and kinetics of their dissolution at pH= 1.0, 3.0, and 6.0 were studied by measurement of the Zn^{2+} concentration. Figure 6a and S7 show the dissolution rate of ZnO QDS at pH 1.0 in which the equilibrium was attained at t≈4 h. For ZnO QDS at pH 1.0, the release of Zn^{2+} ions was around 73% of the theoretical mass. This is in agreement with the TG analysis in which around 25% of the ZnO QDs comprised of the volatile surface functional groups. Consequently, it can be concluded that at pH 1.0, there was a complete dissolution of the ZnO for the bare ZnO QD. To elaborate the extent of dissolution of this QD at different pHs, the UV-Vis absorbance of different solutions after reaching the equilibrium were measured and depicted in Figure 6b. As it can be seen, excitonic peak of ZnO QD at 365 nm disappeared at pH 1.0, due to the complete dissolution of ZnO in such medium. The significantly higher stability of ZnO QDs at pH 3.0 and pH 6.0 is evident in Figure 6b. The quantitative values

of the dissolution rate at different pHs are inserted in Table 2. The bare ZnO QDs as seen are semi-stable at pH 3.0, but quite stable at the higher pH (i.e. 6.0). Figure 6a shows dissolution rate of different samples normalized on the base of their ZnO contents. The applied solution had pH=1. Since according to the TG analysis, ZnO content in ZnO-5% Graphene was around 95%, this sample after dissolution of its ZnO content left 5% of graphene residue. However, for ZnO-30% Graphene dissolution was incomplete; most likely due to the partial wrapping of ZnO QDs by the graphene sheets. In other words, graphene as an impermeable surface provided a barrier against acids for the ZnO QDs. Similar behaviour was reported for PbS-Graphene composite in which around 40% of PbS QDs were remained un-contacted in strong acidic medium [28]. Further evidence for protection effect of graphene can be seen in the UV-Visible spectra of ZnO- 30% Graphene at different pHs in Figure 6d. In contrast to bare ZnO QDs, ZnO-30% Graphene shows the excitonic peak at 365 nm at pH 1.0, implying that higher percentage of graphene results in higher stability of ZnO QDs at acidic medium. Figure S8 in supplementary information depicts the UV-Vis spectra of ZnO-10% Graphene at different pH values.

Figure 6

Table 2

3.5. Precipitation behaviour of the prepared catalysts. The precipitation stability of the synthesized catalysts in DMF and water was examined using time-dependent sedimentation curves (Figure 7). For the bare ZnO QDs dispersion is highly stable because surface organic functional groups act as surfactant, and the A/A_0 ratio (A, extinction at time t; A_0, extinction at time t=0) is nearly constant, with a slight descending slope. Replacing ZnO with graphene in the ZnO-Graphene composite increases the precipitation tendency of the hybrid, as a result of aggregation of graphene sheets with each other. In this respect, it is expected that ZnO-30% Graphene shows a faster sedimentation rate than the ZnO-5% Graphene (Figure 7). The affinity of graphene sheets for aggregation is arisen from the π-π interaction between the adjacent plans.

Figure 7

3.6. Photocatalytic Properties: The UV-visible absorption spectra of ZnO QDs and ZnO-Graphene hybrid with different graphene ratios are shown in Figure 8a. The 372 nm absorption excitation peak of ZnO QDs is corresponding to 3.15 eV band gap. It can be observed that introducing of graphene sheet not only increases intensity of light absorption in the UV region, but also extends the light absorption range into visible area. Figure 8b exhibits a plot of the transformed Kubelka-Munk function as a function of energy of photons, by which the estimated band gaps were found 2.7, 2.8, 2.9, and 3.15 eV for ZnO-30% Graphene, ZnO-10% Graphene, ZnO-5% Graphene, and bare ZnO QDs, respectively. This red shift in the absorption edge of ZnO-Graphene hybrid and consequently visible light activation can be attributed to the chemical bonding between ZnO QDs and the active oxygen-bearing nucleation sites on the surface of GO. In other words, the formation of Zn-O-C bonds between ZnO QDs and graphene as was discussed in the "*connection mechanism*" section, involves the band gap narrowing of ZnO QDs, and broadens the light absorption range of ZnO QDs toward the visible region (Figure 8b). The visible light activation of graphene-based semiconductors due to the chemical connection was reported previously [46-49].

Figure 8

The time-dependent UV–VIS spectra of MO degradation under UV light irradiation are illustrated in Figure S9 in supporting information file. As it can be noticed, the absorbance peak of MO at 464 nm entirely attenuates in 30 min. Figure 9 a, and b show the degradation rate of MO under UV and visible light irradiation for the bare ZnO QDs and the hybrid QDs with different loading of graphene. Figure 9a shows the MO photo-degradation kinetics under UV irradiation fitted by the first-order kinetics model:

$$Ln(\frac{C}{C_0}) = -kt \quad or \quad C = C_0 e^{-kt} \qquad (4)$$

In the absence of catalyst, there is no degradation of the dye in the solution. The photocatalytic efficiency of QDs under both UV and Visible irradiation follows the following order: ZnO-5% Graphene > ZnO-10% Graphene > ZnO QDs > ZnO-30% Graphene. The slope of the ZnO-5% Graphene curve is nearly two times greater than that of the ZnO QDs under UV light irradiation, implying two times faster kinetics at the same condition. In other word, slight introduction of graphene (i.e. 5%) into ZnO catalyst, leads to significant enhancement of its photocatalytic activity. Interestingly, this effect is greater in the visible region, in which the bare ZnO QDs shows a rather low catalytic activity (see discussion below). As shown in Figure 9, in both UV and visible regions, increasing the loading of graphene to 10%, and then 30%, leads to a profound decrease of efficiency of photocatalyst, even lower than ZnO QDs. Probably, at high weight percentage of graphene, it will cover or shade ZnO QDs and decreases their photodegradation efficiency.

As it can be observed in Figure 9b, photocatalytic activity of the ZnO QD is attenuated remarkably under visible light, because its band gap excitation peak lies in the UV region (λ=365 nm)[43]. On the other hand, ZnO-5% Graphene hybrid shows superior photocatalytic activity under visible light region possibly because graphene sheet can: 1) Extend the light absorption of the prepared ZnO-Graphene hybrid into visible light, 2) Efficiently separate photo electron-hole of the ZnO semiconductor, and reduce their recombination rate, and 3) Effectively adsorb the MO molecules and hold them in the vicinity of the ZnO QDs for decomposition. Between the aforementioned three mechanisms, the first one was discussed formerly, and the second will be addressed in the succeeding paragraphs, but the third one needs more clarification as follows. We investigated the adsorption ability of ZnO QDs and ZnO-Graphene composite in dark according to the procedure given in the experimental section, and depicted the results in Figure S10 of supporting information. Evidently, adsorption of MO by ZnO was improved by anchoring of ZnO QDs on the surface of graphene as a result of both π- π interaction between MO molecules and graphene, and high surface area of the graphene sheets[50].

Figure 9

The light absorption, charge transportation, and separation of electron-hole are three important electronic mechanisms of the photocatalysis reaction. The charge transfer and electron-hole separation play significant role in both photocatalytic activity and photocorrosion effect. As it is shown in Figure S11 (Supporting information), ZnO QDs can be excited by UV light and provide electron-hole pairs in which the photo-induced electrons are excited from the valence band (VB) to conduction band (CB) forming a hole in the VB. Because the valence band (VB) position of ZnO QDs is lower than the highest occupied molecular orbital (HOMO) of graphene, the photo-induced holes could transfer to graphene[51]. Such hole transfer increases the lifetime of the free electrons of the ZnO QDs, and reduces their recombination rate with the holes, causing an enhanced level of photocatalytic activity.

Due to wide band gap (3.2 eV), ZnO QDs is not excited by visible light irradiation[52]. Because the conduction band (CB) location of ZnO QDs is lower than the low unoccupied molecular orbital (LUMO) of graphene, the photogenerated electrons by visible light could transfer from graphene sheets to the CB of ZnO QDs. These electrons, then transfer to the surface of photocatalyst and react with water and oxygen resulting in superoxide radicals production (see discussion of S11 figure in Supporting information file). The aforementioned explanation demonstrates that the mechanism of photocatalytic activation of ZnO by Graphene in the case of visible light is different with that of the UV irradiation.

3.7. Photocorrosion Suppression: One of the most important properties of the industrial photocatalysts is that their photocatalytic efficiency should be maintained in the successive cycles of degradation of organic compounds[53]. In this regards, the cyclic experiments for the degradation of MO on ZnO- graphene hybrids were conducted. As shown in Figure 10, under UV irradiation about 80% of MO could be degraded using ZnO QDs for the first time. As it can be seen, after three cycles of usage, a considerable reduction in photocatalytic activity of ZnO QDs

was observed so that only 52% of MO could be decomposed, presumably due to the photocorrostion effect. However, when ZnO surface is covered-passivated by the graphene sheets, ZnO-Graphene composites represent long-lasting photostability. This can be observed in Figure 10 in which photocatalytic activity of ZnO-5% Graphene and ZnO-30% Graphene reduced merely 8% and 2%, respectively, after three recycling experiments.. This photocorrosion inhabitation could be attributed to the close contact between ZnO QDs and graphene sheets through Zn-O-C and Zn-C chemical bonds (See Formation Mechanism Section) which brings about to the graphene its protective effect. The higher photocorrosion suppression of ZnO-30% Graphene compared to ZnO-5% Graphene could be attributed to its higher graphene content. Similar to this results is presented in dissolution stability of ZnO-Graphene composites in which high graphene content protect ZnO QDs at low pH (Figure 6a).

Figure 10

To manifest the effect of photocorrosion phenomena, the absorption peak of ZnO QDs, and ZnO-30% Graphene before and after 24 hr UV irradiation were obtained. As shown in Figure 11a and b, the absorption peak of ZnO QDs almost disappeared after 24 hr photocatalytic activity due to photocorrostion effect, while the absorption peak of ZnO-30% Graphene after 24 hr UV irradiation is nearly identical to its zero irradiation level (Figure 11b). Furthermore, the photocorrostion inhabitation can be examined by measuring Zn^{2+} concentration before and after photocatalytic reaction. Table 3 listed Zn^{2+} ions concentration for ZnO QDs, ZnO-5% Graphene, and ZnO-30% Graphene indicating destruction of ZnO QDs crystal structure in the absence of graphene sheets and releasing more Zn^{2+} ions through the following reaction[53]:

$$ZnO + 2h^{+} + nH_2O \longrightarrow Zn(OH)_n^{(2-n)+} + 0.5O_2 + nH^{+} \qquad (5)$$

where n depends on the pH of the solution. The above mentioned reaction indicates that the photoinduced holes get involved in the photocorrostion of ZnO QDs crystal in aqueous solutions.

As it was mentioned in the previous section, in ZnO-graphene composite, holes are transferred from the ZnO QDs to the graphene sheets, and thus, they are no longer available to corrode the surface of ZnO via the reaction (5) mechanism. In other words, in the absence of water, the photocorrosion effect could be neglected. In this regards, the UV-visible absorbance of ZnO QDs and ZnO-30% Graphene in DMF solution are exhibited in Figure 11c and d, in which there is no difference between absorption peak before and after UV irradiation.

Table 3

Figure 11

4. Conclusions: In summary, we have for the first time tackled the deposition - formation mechanism of the ZnO QDs on the surface of GO which can be used for understanding of the immobilization of other metal oxides on the surface of GO. Integration of the ZnO QDs with graphene brings about three significant outcomes: 1- GO acts as a substrate for nucleation and growth of the ZnO QDs, and at the same time hinders their aggregation. In the absence of such substrate, ZnO QDs tend to agglomerate and produce larger particles. 2- Graphene adsorb the organic molecules and holds them near to ZnO QDs to be degraded by ZnO by different electronic-chemical mechanisms and 3: The electron–hole pairs in the excited ZnO QDs can be efficiently separated through the transport of electrons or to the graphene. As a whole, existence of graphene improves the photocatalytic activity of the ZnO QDs and broaden the absorption range of wavelength toward visible light. Thus the prepared ZnO-Graphene composites show promising photodegradation properties, especially in the visible region. Introduction of graphene sheets not only increases the light absorption of ZnO-Graphene composites, but also produces an activated photocatalysts that *via* extending electron-hole life-time results in efficient oxidation- reduction reaction for degradation of organic pollutants. It has been demonstrated that ZnO-Graphene composites possess antiphotocorrosion properties especially in high loading content of graphene sheets.

The current study synthesized the ZnO-Graphene composite with different loading of graphene, ranging from 5 to 30%, and investigated their various physicochemical properties. Our study showed that although the higher loading of graphene improves acid resistance and precipitation stability of the prepared catalyst, the highest photocatalytic activity is resulted when the amount of the graphene added is slight and around 5%.

Notes: The authors declare no competing financial interest.

Acknowledgments: The authors would like to expresses their gratitude to Ms. Mahnaz separdar for her appreciable discussion on the mechanisms of formation. They are also thankful to Department of Energy Engineering of Sharif University of Technology for financial supports of this project.

*__Supporting Information__ file is available: Raman fitted spectra, TEM images, EDX analysis, Full scan XPS, Up-shifting of Zn2p core level peak, Spectral degradation of MO, Photocatalytic mechanism.

5- References

[1] W. Viessman, M.J. Hammer, E.M. Perez, P.A. Chadik, Water supply and pollution control, Pearson Prentice Hall New Jersey, NJ, 2009.
[2] N. Ghaffour, T.M. Missimer, G.L. Amy, Technical review and evaluation of the economics of water desalination: current and future challenges for better water supply sustainability, Desalination, 309 (2013) 197-207.
[3] A. Pérez-González, A. Urtiaga, R. Ibáñez, I. Ortiz, State of the art and review on the treatment technologies of water reverse osmosis concentrates, Water research, 46 (2012) 267-283.
[4] J. Fang, H. Fan, G. Dong, A facile way to synthesize cost-effective ZnO nanorods with enhanced photocatalytic activity, Materials Letters, 120 (2014) 147-150.
[5] M.R. Hoffmann, S.T. Martin, W. Choi, D.W. Bahnemann, Environmental applications of semiconductor photocatalysis, Chem. Rev., 95 (1995) 69-96.
[6] J. Fang, H. Fan, Y. Ma, Z. Wang, Q. Chang, Surface defects control for ZnO nanorods synthesized by quenching and their anti-recombination in photocatalysis, Applied Surface Science, 332 (2015) 47-54.
[7] H. Yu, H. Fan, X. Wang, J. Wang, Synthesis and characterization of ZnO microstructures via microwave-assisted hydrothermal synthesis process, Optik-International Journal for Light and Electron Optics, 125 (2014) 1461-1464.
[8] R. Lv, X. Wang, W. Lv, Y. Xu, Y. Ge, H. He, G. Li, X. Wu, X. Li, Q. Li, Facile synthesis of ZnO nanorods grown on graphene sheets and its enhanced photocatalytic efficiency, Journal of Chemical Technology & Biotechnology, (2014) n/a-n/a.
[9] S. Banerjee, S.C. Pillai, P. Falaras, K.E. O'Shea, J.A. Byrne, D.D. Dionysiou, New Insights into the Mechanism of Visible Light Photocatalysis, The Journal of Physical Chemistry Letters, 5 (2014) 2543-2554.
[10] C. Han, M.-Q. Yang, N. Zhang, Y.-J. Xu, Enhancing the visible light photocatalytic performance of ternary CdS–(graphene–Pd) nanocomposites via a facile interfacial mediator and co-catalyst strategy, Journal of Materials Chemistry A, (2014).
[11] Z. Liu, Z. Liu, T. Cui, J. Li, J. Zhang, T. Chen, X. Wang, X. Liang, Photocatalysis of two-dimensional honeycomb-like ZnO nanowalls on zeolite, Chemical Engineering Journal, 235 (2014) 257-263.
[12] F.F. de Brites-Nóbrega, A.N.B. Polo, A.M. Benedetti, M.M.D. Leão, V. Slusarski-Santana, N.R.C. Fernandes-Machado, Evaluation of photocatalytic activities of supported catalysts on NaX zeolite or activated charcoal, Journal of Hazardous Materials, 263, Part 1 (2013) 61-66.
[13] H. Tian, H. Fan, H. Guo, N. Song, Solution-based synthesis of ZnO/carbon nanostructures by chemical coupling for high performance gas sensors, Sensors and Actuators B: Chemical, 195 (2014) 147-150.
[14] X. Bai, L. Wang, R. Zong, Y. Lv, Y. Sun, Y. Zhu, Performance Enhancement of ZnO Photocatalyst via Synergic Effect of Surface Oxygen Defect and Graphene Hybridization, Langmuir, 29 (2013) 3097-3105.
[15] N. Song, H. Fan, H. Tian, Reduced graphene oxide/ZnO nanohybrids: Metallic Zn powder induced one-step synthesis for enhanced photocurrent and photocatalytic response, Applied Surface Science, 353 (2015) 580-587.
[16] N. Zhang, Y. Zhang, Y.-J. Xu, Recent progress on graphene-based photocatalysts: current status and future perspectives, Nanoscale, 4 (2012) 5792-5813.
[17] A.K. Geim, K.S. Novoselov, The rise of graphene, Nat Mater, 6 (2007) 183-191.
[18] M. Tayebi, A. Ramazani S.A, M.T. Hamed Mosavian, A. Tayyebi, LDPE/EVA/graphene nanocomposites with enhanced mechanical and gas permeability properties, Polymers for Advanced Technologies, 26 (2015) 1083-1090.
[19] S. Goenka, V. Sant, S. Sant, Graphene-based nanomaterials for drug delivery and tissue engineering, Journal of Controlled Release, 173 (2014) 75-88.
[20] A. Lipatov, A. Varezhnikov, P. Wilson, V. Sysoev, A. Kolmakov, A. Sinitskii, Highly selective gas sensor arrays based on thermally reduced graphene oxide, Nanoscale, 5 (2013) 5426-5434.

[21] B.F. Machado, P. Serp, Graphene-based materials for catalysis, Catalysis Science & Technology, 2 (2012) 54-75.
[22] M. Tavakoli, A. Tayyebi, A. Simchi, H. Aashuri, M. Outokesh, Z. Fan, Physicochemical properties of hybrid graphene–lead sulfide quantum dots prepared by supercritical ethanol, Journal of Nanoparticle Research, 17 (2015) 1-13.
[23] D.R. Dreyer, A.D. Todd, C.W. Bielawski, Harnessing the chemistry of graphene oxide, Chemical Society Reviews, 43 (2014) 5288-5301.
[24] K.A. Mkhoyan, A.W. Contryman, J. Silcox, D.A. Stewart, G. Eda, C. Mattevi, S. Miller, M. Chhowalla, Atomic and Electronic Structure of Graphene-Oxide, Nano Letters, 9 (2009) 1058-1063.
[25] Q. Xiang, J. Yu, M. Jaroniec, Graphene-based semiconductor photocatalysts, Chemical Society Reviews, 41 (2012) 782-796.
[26] M.-Q. Yang, N. Zhang, M. Pagliaro, Y.-J. Xu, Artificial photosynthesis over graphene–semiconductor composites. Are we getting better?, Chemical Society Reviews, 43 (2014) 8240-8254.
[27] A. Tayyebi, M. Outokesh, S. Moradi, A. Doram, Synthesis and characterization of ultrasound assisted "graphene oxide–magnetite" hybrid, and investigation of its adsorption properties for Sr(II) and Co(II) ions, Applied Surface Science, 353 (2015) 350-362.
[28] A. Tayyebi, M.M. Tavakoli, M. Outokesh, A. Shafiekhani, A. Simchi, Supercritical Synthesis and Characterization of Graphene–PbS Quantum Dots Composite with Enhanced Photovoltaic Properties, Industrial & Engineering Chemistry Research, 54 (2015) 7382-7392.
[29] B. Li, H. Cao, ZnO@graphene composite with enhanced performance for the removal of dye from water, Journal of Materials Chemistry, 21 (2011) 3346-3349.
[30] T. Lv, L. Pan, X. Liu, Z. Sun, Enhanced photocatalytic degradation of methylene blue by ZnO-reduced graphene oxide-carbon nanotube composites synthesized via microwave-assisted reaction, Catalysis Science & Technology, 2 (2012) 2297-2301.
[31] J. Jasieniak, M. Califano, S.E. Watkins, Size-Dependent Valence and Conduction Band-Edge Energies of Semiconductor Nanocrystals, ACS Nano, 5 (2011) 5888-5902.
[32] T.J. Jacobsson, T. Edvinsson, Antireflective coatings of ZnO quantum dots and their photocatalytic activity, RSC Advances, 2 (2012) 10298-10305.
[33] D.I. Son, B.W. Kwon, D.H. Park, W.-S. Seo, Y. Yi, B. Angadi, C.-L. Lee, W.K. Choi, Emissive ZnO-graphene quantum dots for white-light-emitting diodes, Nat Nano, 7 (2012) 465-471.
[34] M.-C. Hsiao, S.-H. Liao, M.-Y. Yen, P.-I. Liu, N.-W. Pu, C.-A. Wang, C.-C.M. Ma, Preparation of Covalently Functionalized Graphene Using Residual Oxygen-Containing Functional Groups, ACS Applied Materials & Interfaces, 2 (2010) 3092-3099.
[35] X. Wang, S.M. Tabakman, H. Dai, Atomic Layer Deposition of Metal Oxides on Pristine and Functionalized Graphene, Journal of the American Chemical Society, 130 (2008) 8152-8153.
[36] Q. Ma, X. Zhu, D. Zhang, S. Liu, Graphene oxide - a surprisingly good nucleation seed and adhesion promotion agent for one-step ZnO lithography and optoelectronic applications, Journal of Materials Chemistry C, 2 (2014) 8956-8961.
[37] W.S. Hummers, R.E. Offeman, Preparation of Graphitic Oxide, Journal of the American Chemical Society, 80 (1958) 1339-1339.
[38] S. Moradi, O. Akhavan, A. Tayyebi, R. Rahighi, M. Mohammadzadeh, H.S. Rad, Magnetite/dextran-functionalized graphene oxide nanosheets for in vivo positive contrast magnetic resonance imaging, RSC Advances, 5 (2015) 47529-47537.
[39] P.K. Ang, S. Wang, Q. Bao, J.T.L. Thong, K.P. Loh, High-Throughput Synthesis of Graphene by Intercalation−Exfoliation of Graphite Oxide and Study of Ionic Screening in Graphene Transistor, ACS Nano, 3 (2009) 3587-3594.
[40] S.F. Yu, C. Yuen, S.P. Lau, W.I. Park, G.-C. Yi, Random laser action in ZnO nanorod arrays embedded in ZnO epilayers, Applied Physics Letters, 84 (2004) 3241-3243.

[41] S. Webster, R. Czerw, D. Carroll, M. Terrones, N. Grobert, Raman Study of Doped Multiwalled Carbon Nanotubes, in: APS Meeting Abstracts, 2002, pp. 25011.
[42] A. Nourmohammadi, R. Rahighi, O. Akhavan, A. Moshfegh, Graphene oxide sheets involved in vertically aligned zinc oxide nanowires for visible light photoinactivation of bacteria, Journal of Alloys and Compounds, 612 (2014) 380-385.
[43] O. Akhavan, Photocatalytic reduction of graphene oxides hybridized by ZnO nanoparticles in ethanol, Carbon, 49 (2011) 11-18.
[44] D. Rosenthal, M. Ruta, R. Schlögl, L. Kiwi-Minsker, Combined XPS and TPD study of oxygen-functionalized carbon nanofibers grown on sintered metal fibers, Carbon, 48 (2010) 1835-1843.
[45] D. Yang, A. Velamakanni, G. Bozoklu, S. Park, M. Stoller, R.D. Piner, S. Stankovich, I. Jung, D.A. Field, C.A. Ventrice Jr, R.S. Ruoff, Chemical analysis of graphene oxide films after heat and chemical treatments by X-ray photoelectron and Micro-Raman spectroscopy, Carbon, 47 (2009) 145-152.
[46] H. Zhang, X. Lv, Y. Li, Y. Wang, J. Li, P25-graphene composite as a high performance photocatalyst, ACS nano, 4 (2009) 380-386.
[47] H.N. Tien, N.T. Khoa, S.H. Hahn, J.S. Chung, E.W. Shin, S.H. Hur, One-pot synthesis of a reduced graphene oxide–zinc oxide sphere composite and its use as a visible light photocatalyst, Chemical Engineering Journal, 229 (2013) 126-133.
[48] N. Zhang, M.-Q. Yang, S. Liu, Y. Sun, Y.-J. Xu, Waltzing with the Versatile Platform of Graphene to Synthesize Composite Photocatalysts, Chemical reviews, 115 (2015) 10307-10377.
[49] Y. Zhang, Z.-R. Tang, X. Fu, Y.-J. Xu, TiO2− graphene nanocomposites for gas-phase photocatalytic degradation of volatile aromatic pollutant: is TiO2− graphene truly different from other TiO2− carbon composite materials?, ACS nano, 4 (2010) 7303-7314.
[50] J. Wang, T. Tsuzuki, B. Tang, X. Hou, L. Sun, X. Wang, Reduced Graphene Oxide/ZnO Composite: Reusable Adsorbent for Pollutant Management, ACS Applied Materials & Interfaces, 4 (2012) 3084-3090.
[51] Y. Wang, R. Shi, J. Lin, Y. Zhu, Enhancement of photocurrent and photocatalytic activity of ZnO hybridized with graphite-like C 3 N 4, Energy & Environmental Science, 4 (2011) 2922-2929.
[52] H. Zhang, R. Zong, Y. Zhu, Photocorrosion inhibition and photoactivity enhancement for zinc oxide via hybridization with monolayer polyaniline, The Journal of Physical Chemistry C, 113 (2009) 4605-4611.
[53] L. Zhang, H. Cheng, R. Zong, Y. Zhu, Photocorrosion suppression of ZnO nanoparticles via hybridization with graphite-like carbon and enhanced photocatalytic activity, The Journal of Physical Chemistry C, 113 (2009) 2368-2374.

Figure Captions

Figure1: (a) A typical AFM image of GO sheet on mica and height profile analysis of marked-line, (b) TEM image of GO sheet , inset demonstrating SAED pattern of GO, and (c) UV-visible absorbance of GO solution (inset optical picture of GO solution)

Figure2: Low magnification TEM image of ZnO-Graphene hybrid, inset corresponding SAED patterns of ZnO QDs and graphene, (b) HR-TEM image of ZnO-Graphene, inset HR-TEM image of single crystal of ZnO QDs, and (c) HR-TEM image of ZnO-Graphene hybrid in which Graphene sheets covered ZnO QDs (Left)

Figure3: (a) Raman spectra of synthesized materials, (b), Thermogravimetric analysis of prepared materials, (c) FTIR patterns of GO and ZnO-Graphene, and (d) The full survey XPS spectra of GO and ZnO-Graphene hybrid.

Figure4: XPS curve fitting of C1s spectra of (a) GO, and (b) ZnO-Graphene.

Figure5: XPS curve fitting of O1s spectra of (a) GO, (b) ZnO-Graphene, and (c) Schematic illustration of Zn^{2+} connection to oxygen functionalities on the surface of GO.

Figure6: (a) Time-dependent measurements of ZnO QDs and ZnO-Graphene dissolution based on Normalized ZnO content at different pH, (b) UV-visible absorbance of ZnO QDs solution after reaching to equilibrium , and (c) UV-visible absorbance of ZnO-30% Graphene solution after reaching to equilibrium (100 mg/L initial mass of ZnO QDs and ZnO Graphene)

Figure7: Sedimentation plot of ZnO QDs, and ZnO-Graphene hybrid in (a) DMF , and (b) Water (pH 7)

Figure 8: UV-Visible absorbance of ZnO QDs and ZnO-Graphene, and (b) The plot of transformed Kubelka-Munk function versus the energy of light.

Figure 9: Kinetic of photocatalytic degradation of MO under (a) UV and (b) Visible light irradiation for ZnO QDs and ZnO-Graphene hybrid.

Figure 10: The photostability of ZnO QDs and ZnO-Graphene composites by investigation of photocatalytic activity under UV irradiation, (Red circle = ZnO QDs, Green triangle = ZnO-30% Graphene, Blue Star = ZnO-5% Graphene).

Figure 11: UV-Visible absorbance of (a) ZnO QDs, (b) ZnO-30% Graphene in aquous solution, (c) ZnO QDs, and (d) ZnO-30% Graphene in DMF solution before and after 24 UV irradiation.

Table

Table 1: Surface concentration of carbon-bonded groups of GO and ZnO-Graphene, calculated from peak areas of the C1s spectra.

Sample	Peaks Area Percentage					
	C-Zn	C=C	C-O-Zn	C-O	C=O	C/O Ratio
GO	0	57	0	33	10	2.3
ZnO-5% Graphene	6	52	25	7	6	7.6

Table 2: Zn^{2+} ions concentration at effluent solution of ZnO QDs and ZnO-Graphene hybrid at different pH.

Type of Catalyst	pH=1 (mg/L)	pH=3 (mg/L)	pH=6 (mg/L)	pH=7.2 (mg/L)
ZnO QDs	74	23	3.1	0.0
ZnO-5% Graphene	69	19	0.3	0.0
ZnO-30% Graphene	34	5	0.15	0.0

Table 3: The concentration of Zn^{2+} ions in the solution of ZnO QDs and ZnO-Graphene photocatalytic process before and after UV irradiation (pH=6.5).

Type of Catalyst	Before UV irradiation (mg/L)	After 24 hr UV irradiation (mg/L)
ZnO QDs	1.4	71
ZnO-5% Graphene	0.2	2.9
ZnO-30% Graphene	0.05	1.3

Figure

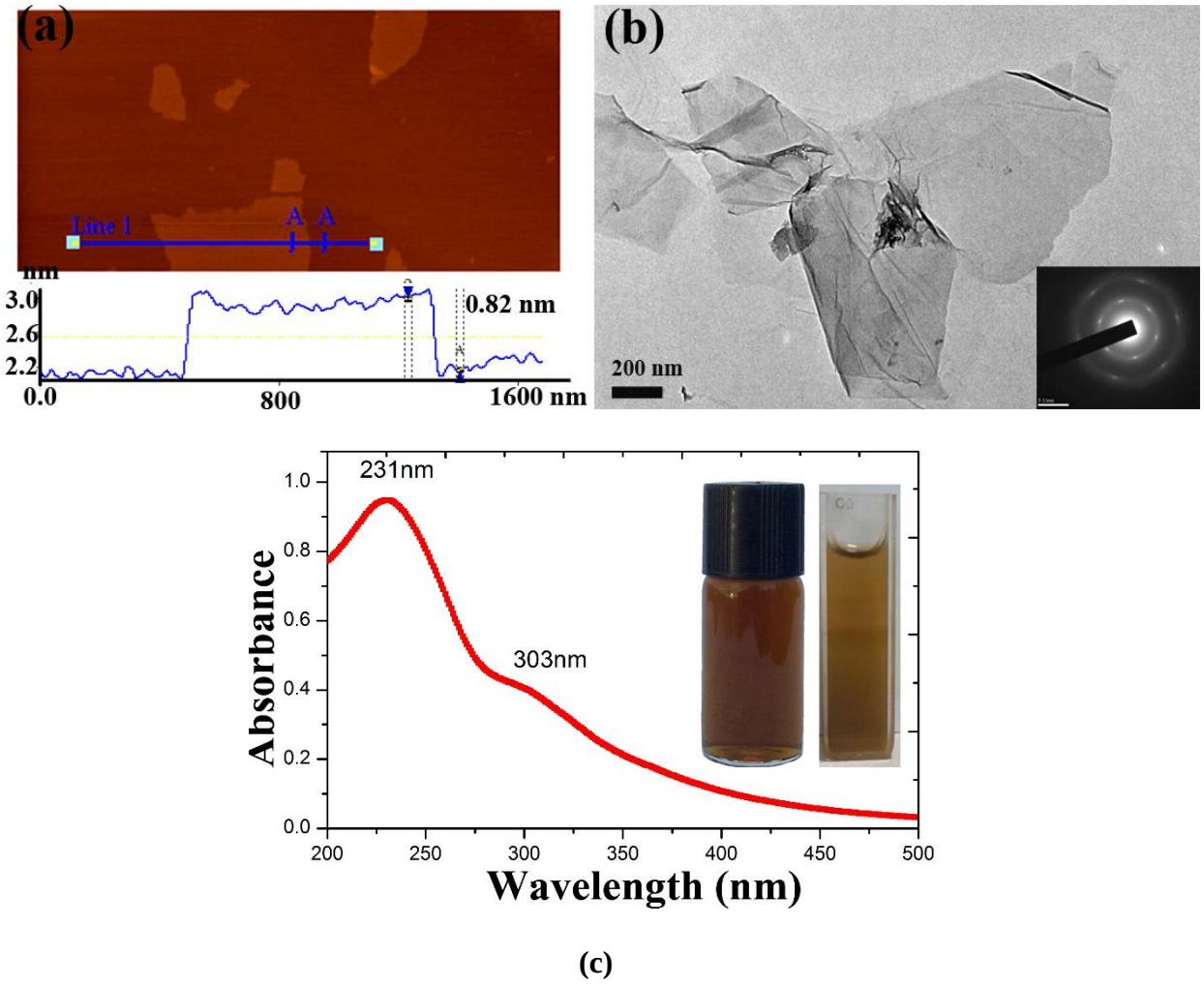

(c)

Figure1: (a) A typical AFM image of GO sheet on mica and height profile analysis of marked-line, (b) TEM image of GO sheet , inset demonstrating SAED pattern of GO, and (c) UV-visible absorbance of GO solution (inset optical picture of GO solution).

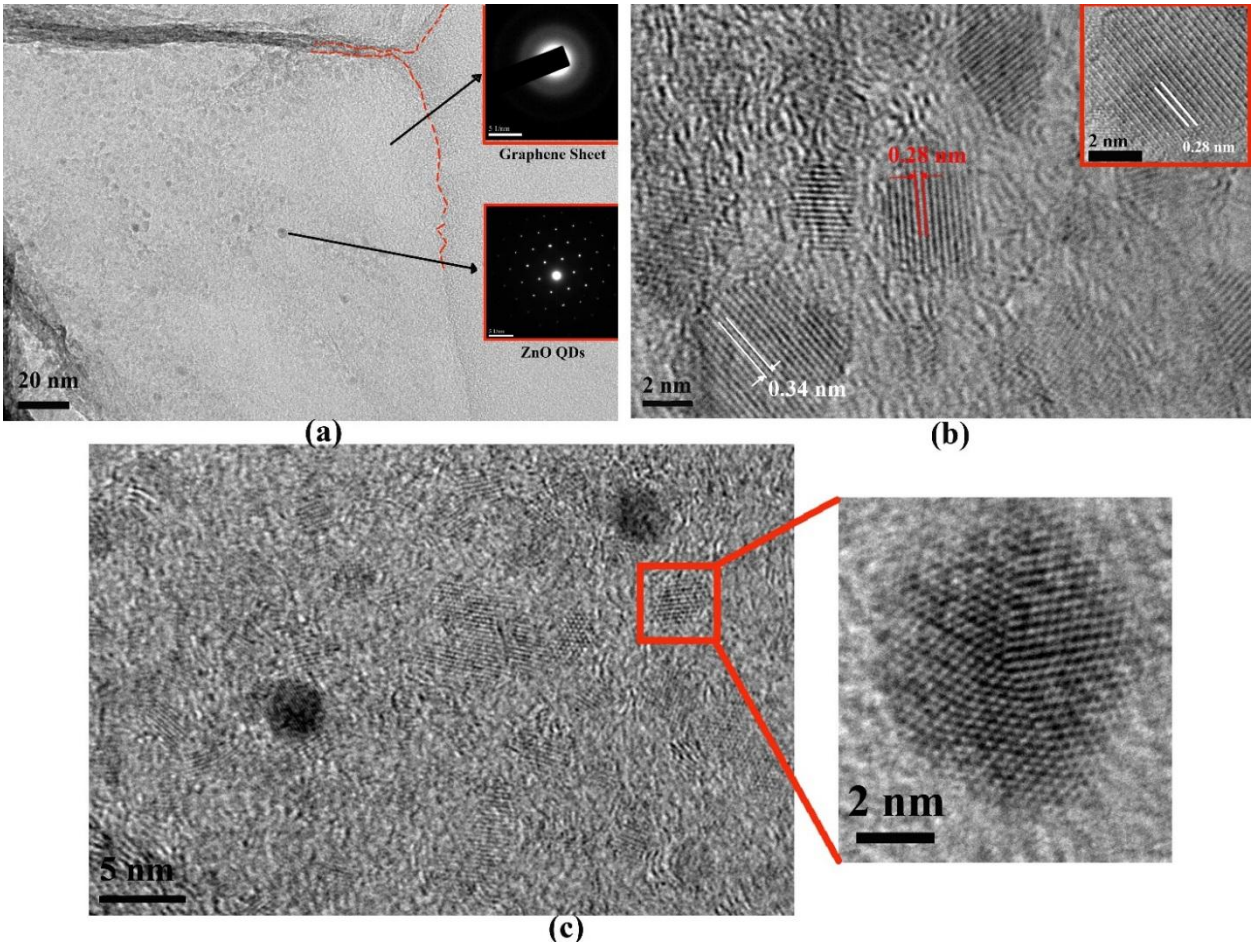

Figure2: Low magnification TEM image of ZnO-Graphene hybrid, inset corresponding SAED patterns of ZnO QDs and graphene, (b) HR-TEM image of ZnO-Graphene, inset HR-TEM image of single crystal of ZnO QDs, and (c) HR-TEM image of ZnO-Graphene hybrid in which Graphene sheets covered ZnO QDs (Left).

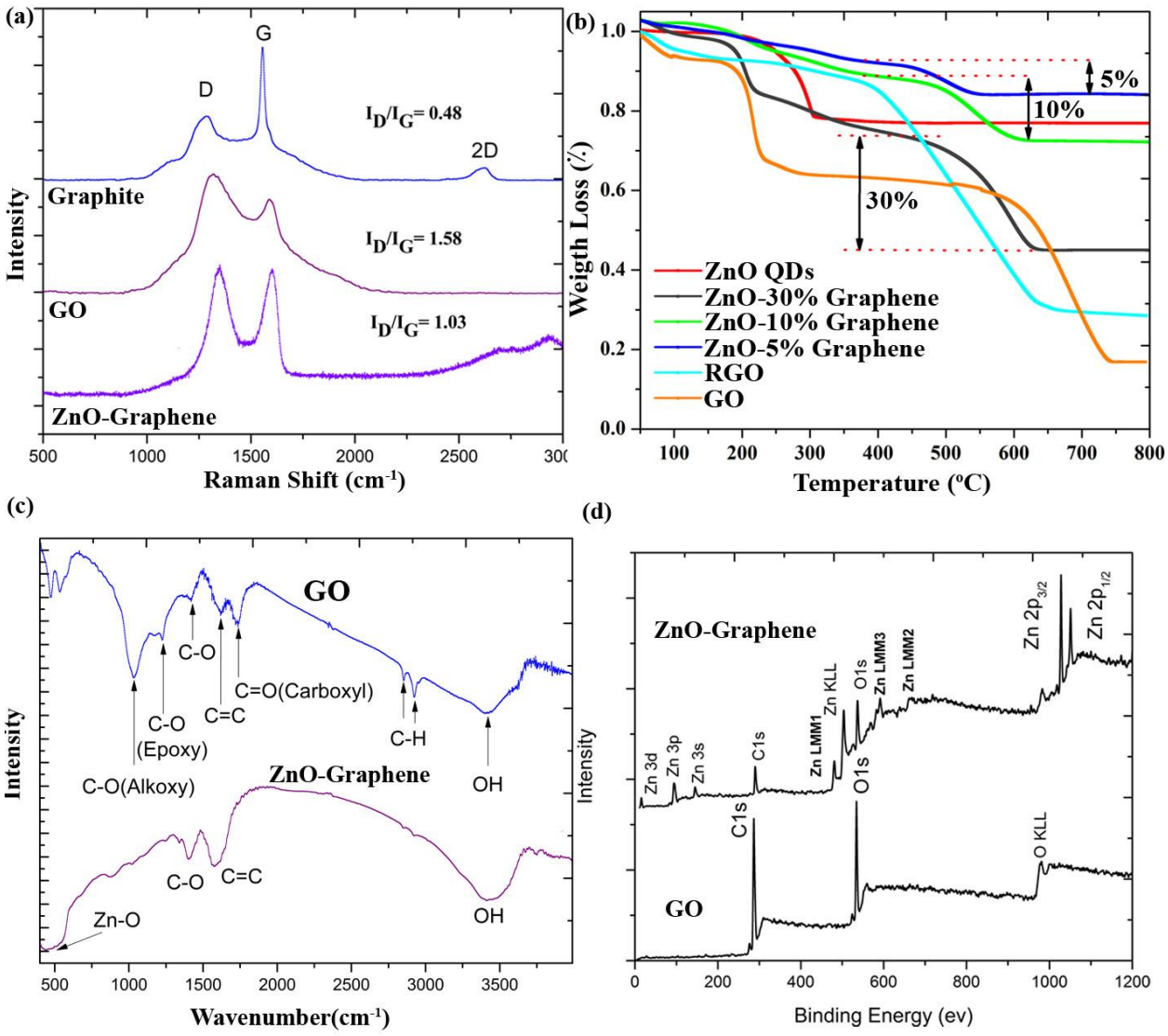

Figure3: (a) Raman spectra of synthesized materials, (b), Thermogravimetric analysis of prepared materials, (c) FTIR patterns of GO and ZnO-Graphene, and (d) The full survey XPS spectra of GO and ZnO-Graphene hybrid.

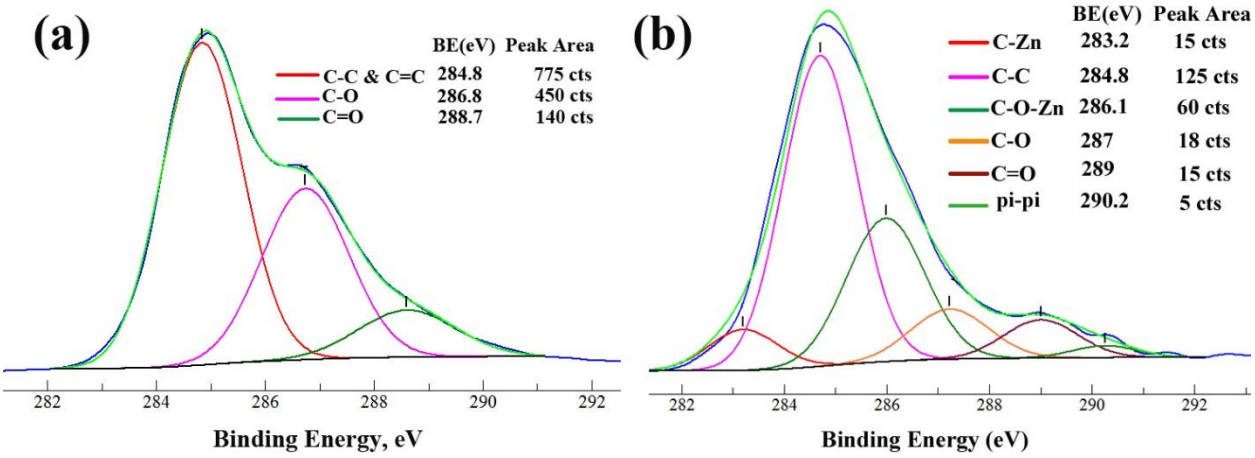

Figure4: XPS curve fitting of C1s spectra of (a) GO, and (b) ZnO-Graphene.

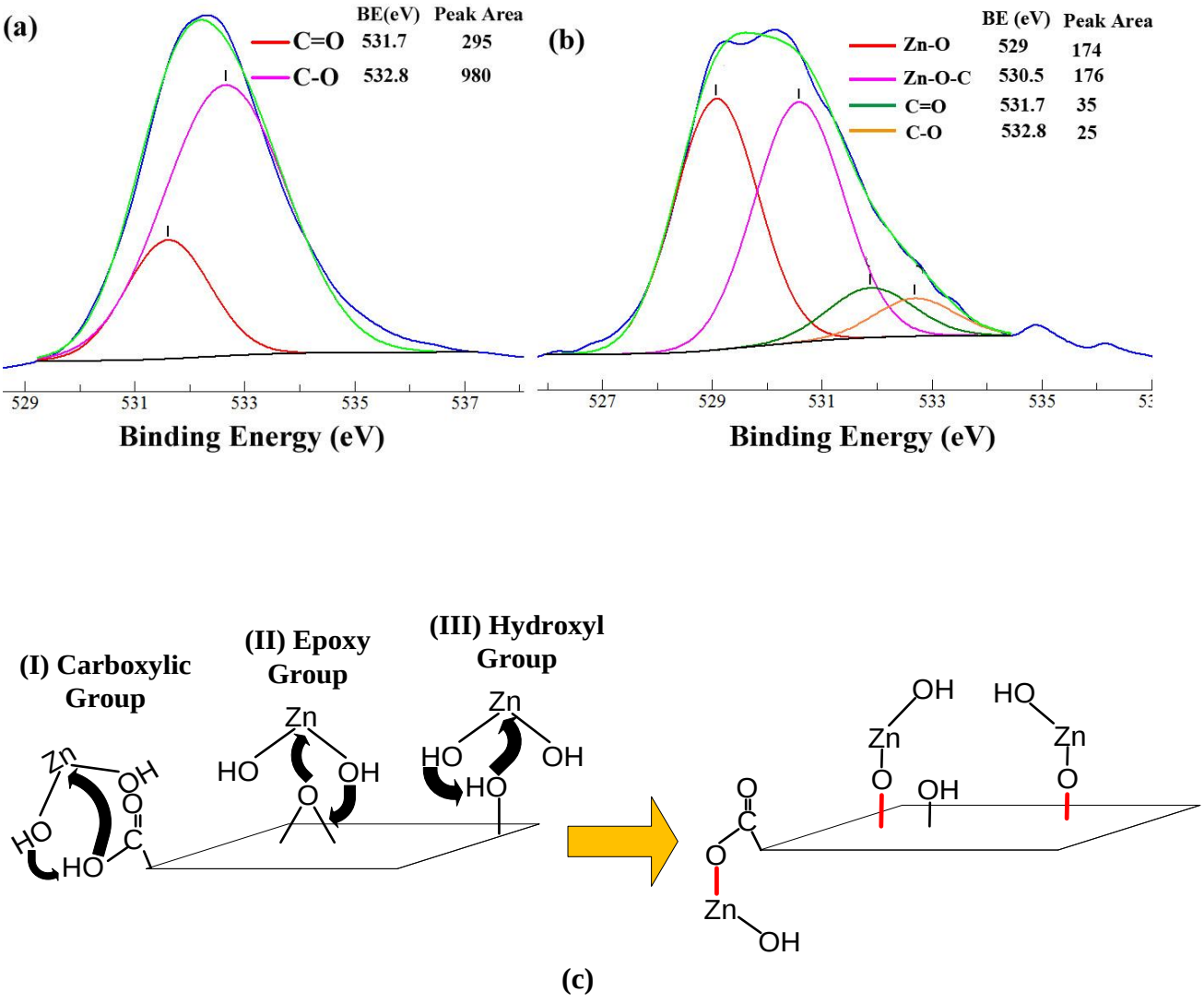

Figure5: XPS curve fitting of O1s spectra of (a) GO, (b) ZnO-Graphene, and (c) Schematic illustration of Zn^{2+} connection to oxygen functionalities on the surface of GO.

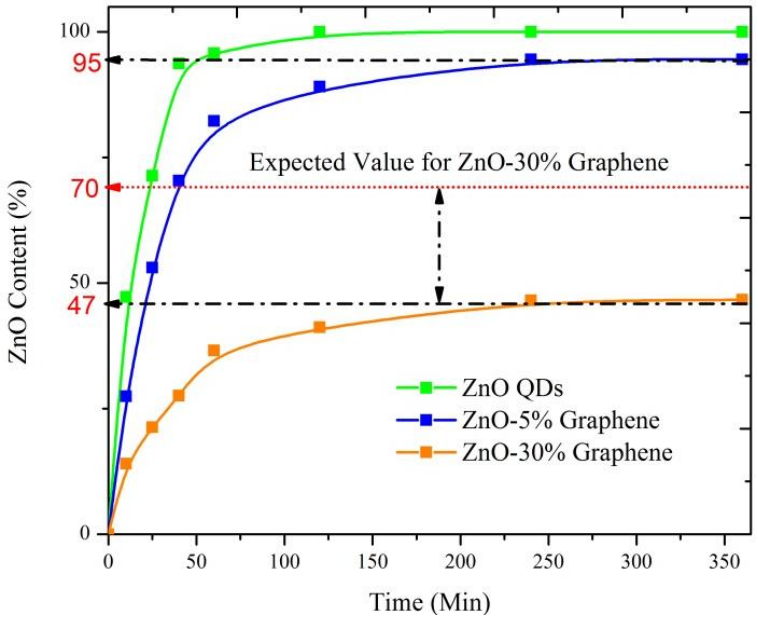

(a)

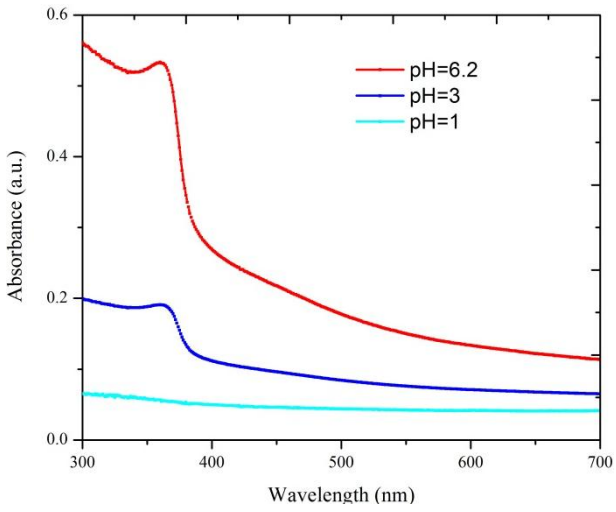

(b)

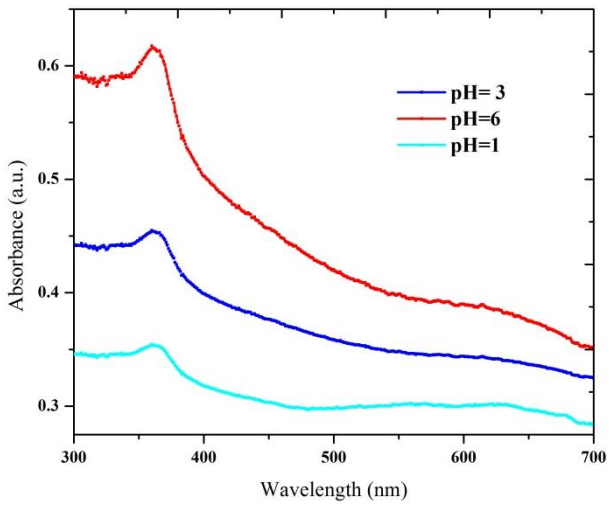

(c)

Figure6: (a) Time-dependent measurements of ZnO QDs and ZnO-Graphene dissolution based on Normalized ZnO content at pH=1, (b) UV-visible absorbance of ZnO QDs solution after reaching to equilibrium , and (c) UV-visible absorbance of ZnO-30% Graphene solution after reaching to equilibrium (100 mg/L initial mass of ZnO QDs and ZnO Graphene).

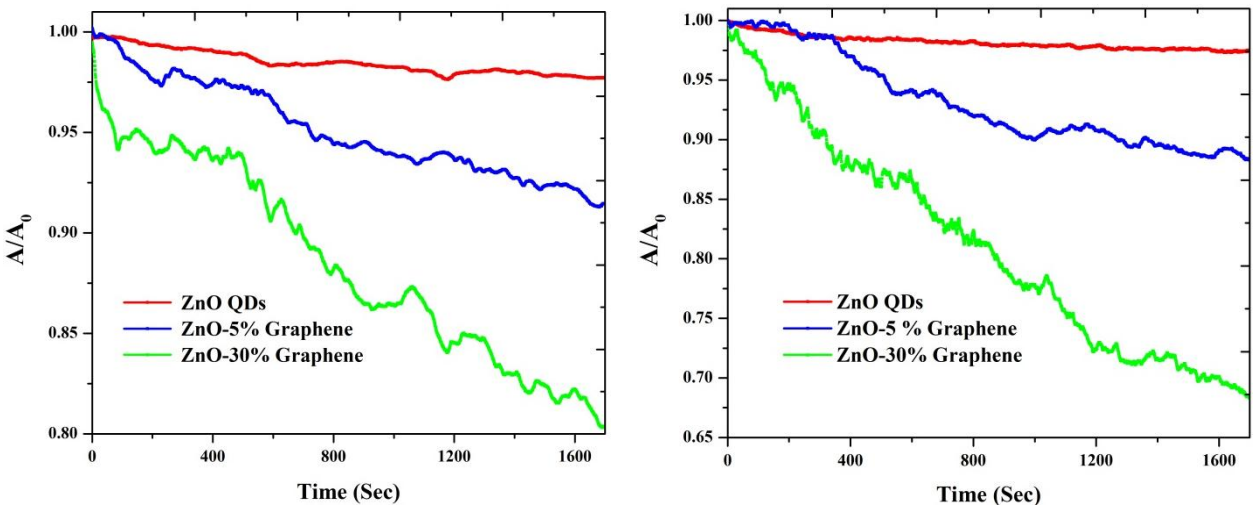

(a) (b)

Figure7: Sedimentation plot of ZnO QDs, and ZnO-Graphene hybrid in (a) DMF , and (b) Water.

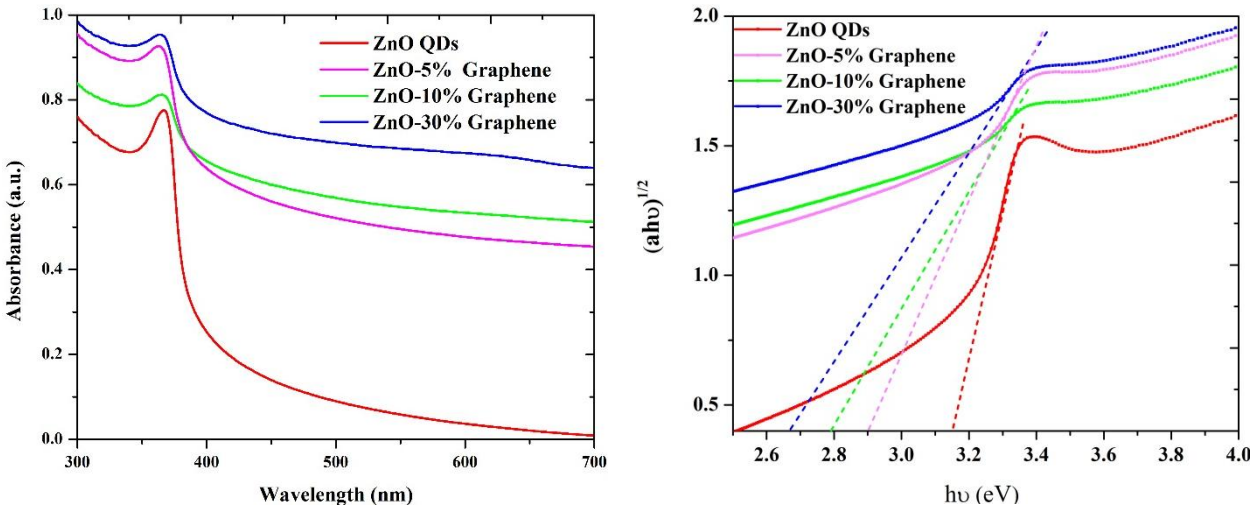

(a) (b)

Figure 8: (a) UV-Visible absorbance of ZnO QDs and ZnO-Graphene, and (b) The plot of transformed Kubelka-Munk function versus the energy of light.

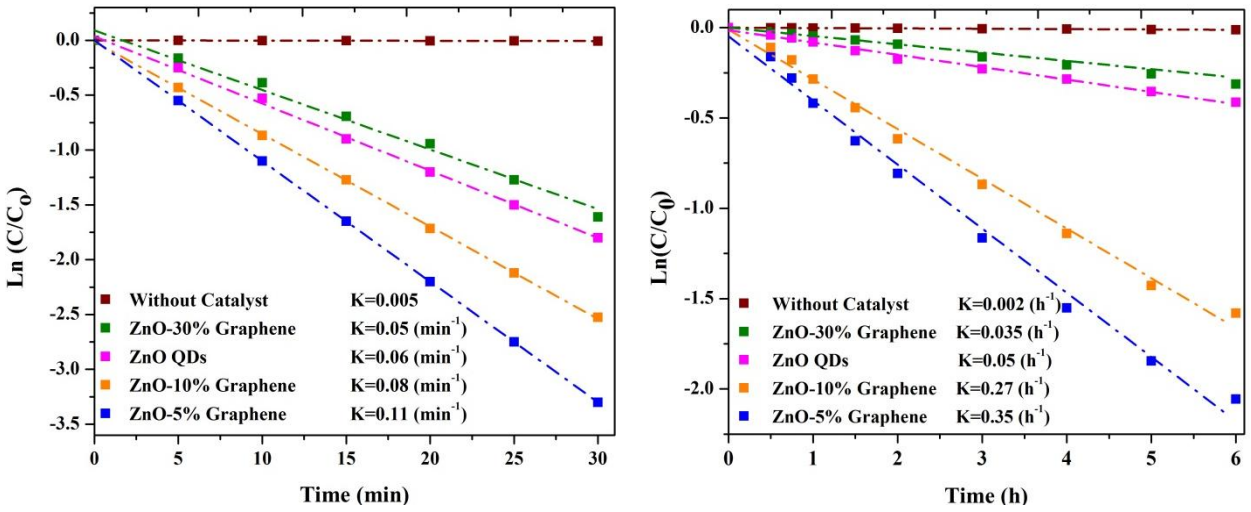

(a) (b)

Figure 9: Kinetic of photocatalytic degradation of MO under (a) UV and (b) Visible light irradiation for ZnO QDs and ZnO-Graphene hybrid.

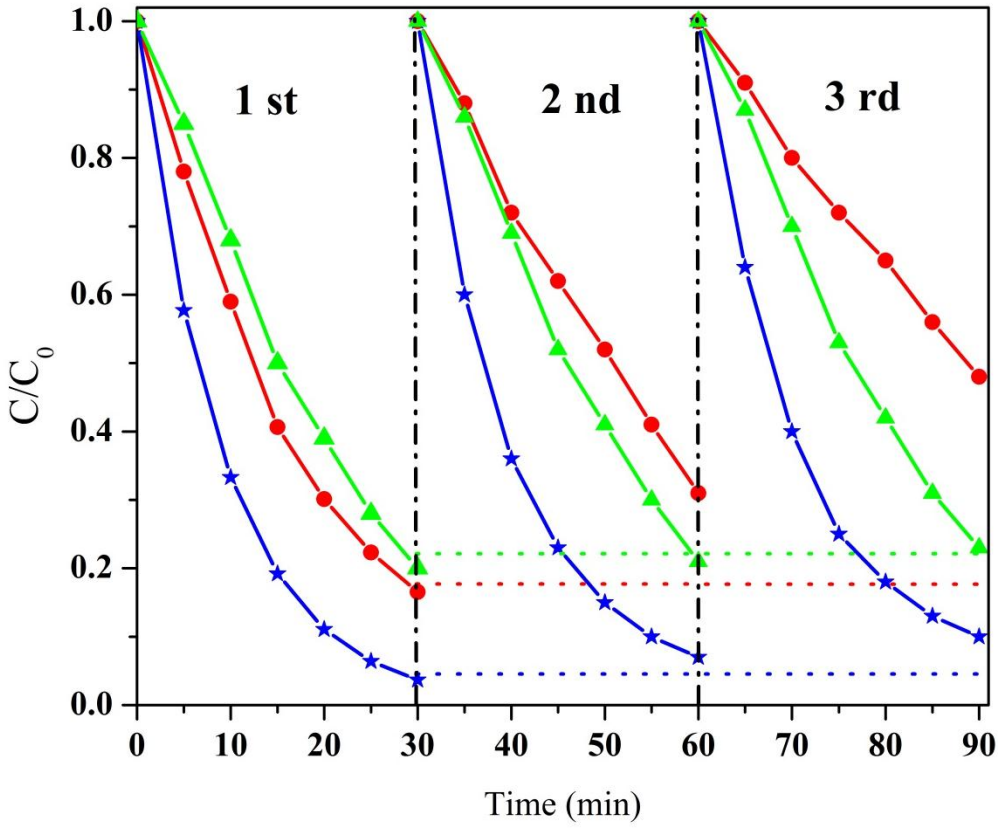

Figure 10: The photostability of ZnO QDs and ZnO-Graphene composites by investigation of photocatalytic activity under UV irradiation, (Red circle = ZnO QDs, Green triangle = ZnO-30% Graphene, Blue Star = ZnO-5% Graphene) .

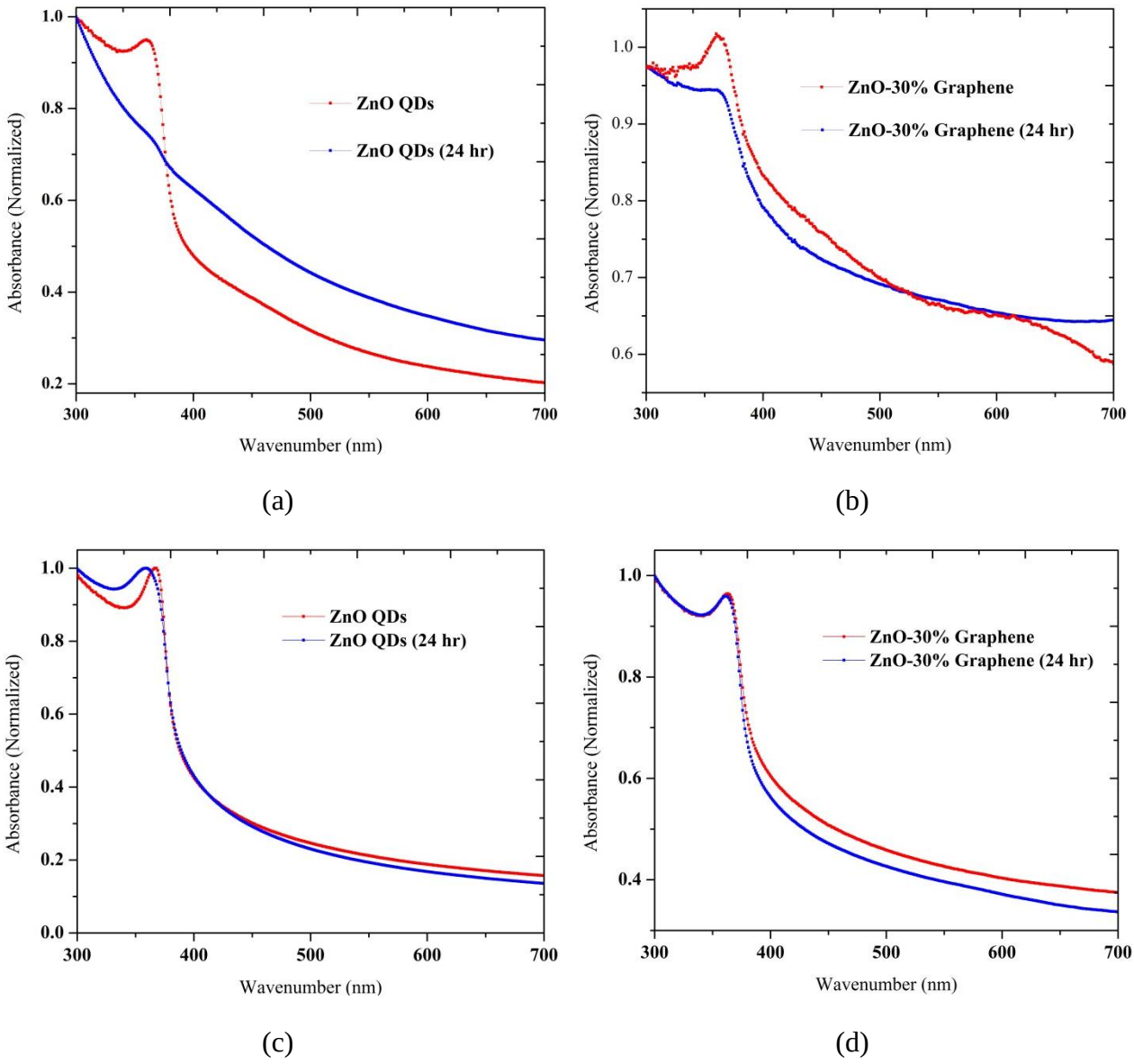

Figure 11: UV-Visible absorbance of (a) ZnO QDs, (b) ZnO-30% Graphene in aquous solution, (c) ZnO QDs, and (d) ZnO-30% Graphene in DMF solution before and after 24 UV irradiation.

Graphical Abstract (for review)

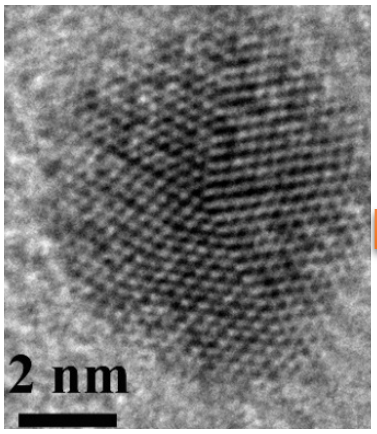

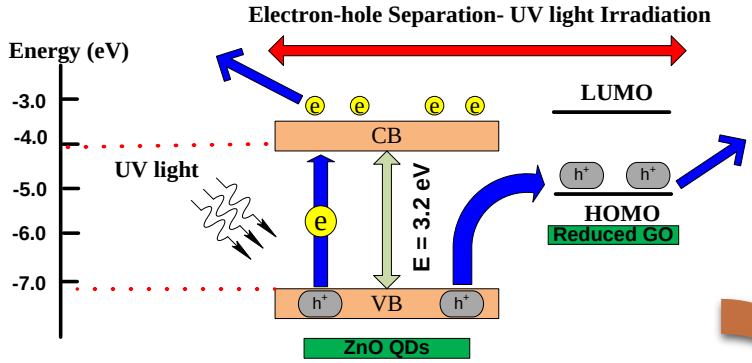

ZnO-Graphene Quantum Dots

Electron-hole Separation Mechanism

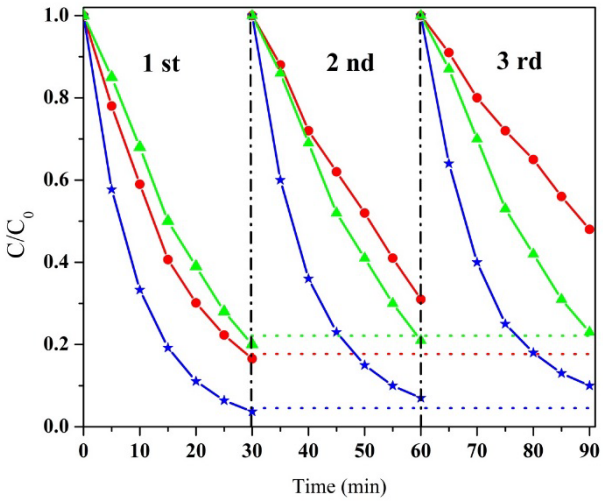

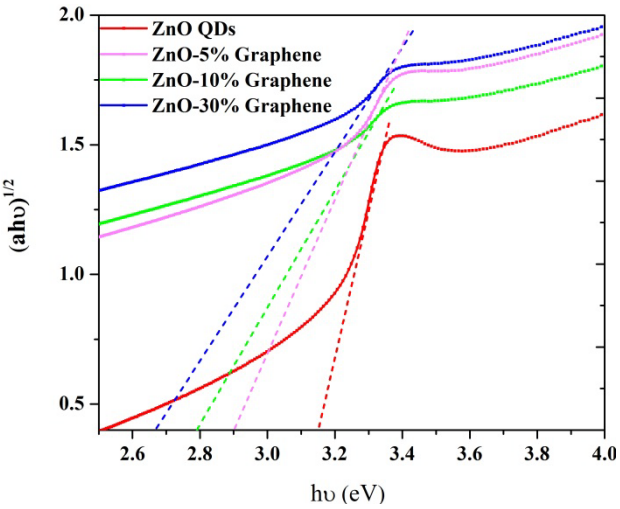

Photocorossion Suppresion of ZnO QDs

Visible light activation of ZnO-Graphene